THE JOURNAL OF PHYSICAL CHEMISTRY B

Article

pubs.acs.org/JPCB

Electrophoretic Nanotechnology of Composite Electrodes for Electrochemical Supercapacitors

Y. Su and I. Zhitomirsky*

Department of Materials Science and Engineering, McMaster University, 1280 Main Street, West Hamilton, Ontario, Canada L8S 4L7

ABSTRACT: The electrophoretic deposition (EPD) method has been developed for the fabrication of MnO_2−multiwalled carbon nanotube (MWCNT) films for application in electrochemical supercapacitors (ESs). For MWCNT applications, which depend on electrical conductivity, it is challenging to achieve dispersion and EPD of pristine MWCNT and avoid defects due to chemical treatment or functionalization. An important finding was the possibility of efficient dispersion and controlled EPD of MWCNT using calconcarboxylic acid (CCA). Moreover, the use of CCA allowed efficient dispersion of MnO_2 in concentrated suspensions and EPD of MnO_2 films. The comparison of the experimental data for chromotrope FB (CFB) and CCA and chemical structures of the molecules provided insight into the mechanism of CCA adsorption on MnO_2. The fabrication of stable suspensions of MnO_2 nanoparticles containing MWCNT, and controlled codeposition of both materials is a crucial aspect in the EPD of composites. The new approach was based on the use of CCA as a charging and dispersing agent for EPD of MnO_2 nanoparticles and MWCNT. The deposition yield measurements at various experimental conditions and Fourier transform infrared spectroscopy data, coupled with results of electron microscopy, thermogravimetric, and differential thermal analysis provided evidence of the formation of MnO_2−MWCNT composites. The electrochemical testing results and impedance spectroscopy data showed good capacitive behavior of the composite films and the beneficial effect of MWCNTs.

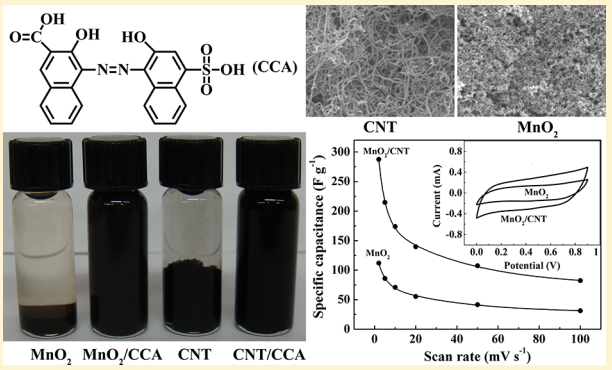

1. INTRODUCTION

Electrophoretic deposition (EPD) is an important colloidal technique for the fabrication of inorganic, polymer, and composite films for electronic, catalytic, biomedical, energy storage, and other applications.[1−4] EPD is achieved via motion of charged particles in a suspension under an applied electric field, followed by particle coagulation and deposition at the electrode surface.[5,6] Bath compositions for EPD included various additives, which provided effective stabilization and charging of inorganic particles in the suspensions.[7,8] Many fundamental studies were focused on the investigation of mechanisms of particle charging and electrophoretic behavior.[9,10]

EPD technology has faced a new challenge with increasing interest in nanostructured materials.[11,12] The dispersion of nanoparticles in suspensions presents difficulties, attributed to their high surface area and strong tendency for agglomeration. It was found that particle size reduction introduced problems related to electric field-induced agglomeration during EPD.[13] Moreover, stirring of suspensions containing very fine particles promoted their agglomeration and sedimentation, which reduced the EPD yield.[13]

Despite the impressive progress achieved in the EPD of various materials, there is a need for simple and versatile methods for efficient chemical modification, dispersion, charging, and deposition of colloidal nanoparticles. The chemical interactions of inorganic nanoparticles with charging or dispersing agents are especially important and must be well understood to predict the adsorption mechanism and dispersion efficiency.[14]

There is increasing interest in the EPD of nanocomposites, combining advanced functional properties of oxide nanoparticles and carbon nanotubes (CNTs).[15−17] EPD is especially attractive for the fabrication of MnO_2−CNT composites for application in electrochemical supercapacitors (ESs). The interest in application of MnO_2 for electrodes of ESs is attributed to high specific capacitance (SC) of this material. However, difficulties are attributed to the dispersion of MnO_2 nanoparticles and fabrication of suspensions of sufficient concentration[18] for application in EPD. CNTs are usually added to MnO_2 in order to increase the electronic conductivity of the composite electrodes and improve the power density of ESs.[19] The use of CNTs as conductive additives offers benefits of their high surface area and low percolation threshold. However, the SC of CNTs is low. Therefore, the fabrication of

Special Issue: Electrophoretic Deposition

Received: May 5, 2012
Revised: May 31, 2012
Published: June 4, 2012

MnO_2−CNT electrodes requires efficient dispersion of CNTs and optimization of the CNT content in the composites.

Various methods have been developed for the dispersion and EPD of CNTs. It was found that adsorbed anionic and cationic polyelectrolytes provided efficient charging of CNT in suspensions and allowed the formation of anodic or cathodic deposits by EPD.[20] Significant effort has been invested in the development of functionalization strategies, which included both covalent and supramolecular approaches.[21,22] However, polymer "wrapping" and supramolecular dispersion methods often result in the formation of CNT bundles.[20,23]

The interactions of CNTs with charging additives and solvents are especially important for EPD technology.[16] Many attempts have been made to improve wetting properties of CNTs in solvents by oxidation in strong acids or mixtures of acids.[23−25] It was shown that under acidic conditions, defective sites in the CNT are attacked, resulting in the formation of fragmented CNT, decorated with carboxylic and other oxygen-containing groups on their surface. These acidic groups electrostatically stabilized the CNT in suspensions and provided a negative charge for EPD.[16] However, the oxidation and functionalization strategies introduce defects on the CNT sidewalls and reduce electronic conductivity of CNT. In another approach, the charging of CNT for EPD was achieved by adsorption of metal ions from added metal salts.[16,26,27] It should be noted that the addition of metal salts results in lower suspension stability, attributed to increasing ionic strength of the suspension. The metal ions usually incorporate into the cathodic deposits as corresponding hydroxides and contaminate the deposits. However, metal hydroxides[28] or polymers[29] incorporated into the deposits provided improved film adhesion, due to their binding properties.

The problems related to the EPD of CNT and composites were addressed in our investigation. The goal of this investigation was the EPD of MnO_2−multiwalled CNT (MWCNT) composite electrodes for applications in ES. The new approach was based on the use of an aromatic surfactant for dispersion and charging of MWCNT. The results presented below showed that good suspension stability and high deposition rate can be achieved using calconcarboxylic acid (CCA). The important finding was the possibility of fabrication of stable concentrated suspensions of MnO_2 nanoparticles and their efficient EPD using CCA as a dispersing and charging agent. The comparison of the chemical structures of chromotrope FB (CFB) and CCA and corresponding experimental data for both molecules provided important insight into the mechanism of CCA adsorption on MnO_2 particles. The key advantage of using CCA was the possibility of efficient dispersion and deposition of two different materials: MWCNT and MnO_2. The ability to control the deposit composition and microstructure allowed the formation of efficient MnO_2−MWCNT nanocomposite for electrodes of ES.

2. EXPERIMENTAL PROCEDURES

CFB, CCA, $KMnO_4$ (Aldrich), and MWCNT (Arkema) were used as starting materials. MnO_2 nanoparticles with an average particle size of 30 nm were prepared by the reduction method[30] using aqueous $KMnO_4$ solutions and ethanol as a reducing agent. Electrophoretic deposits were obtained on stainless steel substrates (50 × 50 mm) from suspensions, containing 0−1 g L^{-1} MWCNT and 0−10 g L^{-1} MnO_2 in ethanol. The concentration of CFB and CCA in the suspensions was varied in the range of 0−1 g L^{-1}. Before the deposition, the suspensions were ultrasonicated for 30 min to achieve a homogeneous dispersion. The deposition was performed at constant voltages of 10−70 V. The distance between the substrates and platinum counter electrodes was 15 mm. The deposition time was varied in the range of 0−10 min. After deposition, the deposits were dried in air for 48 h.

The deposits were removed from the substrates for the Fourier transform infrared spectroscopy (FTIR), thermogravimetric analysis (TGA) and differential thermal analysis (DTA). FTIR studies were performed using Bio-Rad FTS-40 instrument. The TGA and DTA investigations were carried out in air at a heating rate of 5 °C min^{-1} using a thermoanalyzer (Netzsch STA-409). The microstructure of the films was investigated using a JEOL JSM-7000F scanning electron microscope (SEM). Electrochemical studies were performed using a potentiostat (PARSTAT 2273, Princeton Applied Research). Surface area of the working electrode was 1 cm^2. The counter electrode was a platinum gauze, and the reference electrode was a standard calomel electrode (SCE). Capacitive behavior and electrochemical impedance of the films were investigated in 0.5 M Na_2SO_4 aqueous solutions. Cyclic voltammetry (CV) studies were performed within a potential range of 0−0.9 V versus SCE at scan rates of 2−100 mVs^{-1}. The SC was calculated using half the integrated area of the CV curve to obtain the charge (Q), and subsequently dividing the charge by the film mass (m) and width of the potential window (ΔV):

$$C = \frac{Q}{m\Delta V} \quad (1)$$

Impedance spectroscopy investigations were performed in the frequency range of 0.1 Hz to 100 kHz, the amplitude of the applied voltage was 5 mV.

3. RESULTS AND DISCUSSION

Figure 1A,B compares structures of CFB and CCA used in this investigation. CFB and CCA are aromatic compounds with

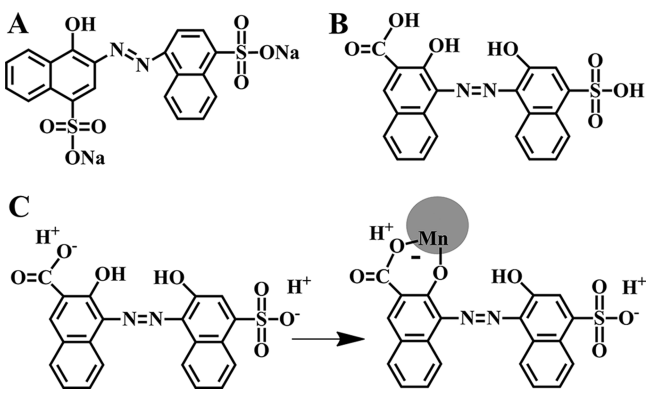

Figure 1. (A) Chemical structure of CFB, (B) chemical structure of CCA, and (C) mechanism of CCA adsorption on MnO_2 particles.

conjugated bonds. The anionic properties of CFB (Figure 1A) are related to SO_3^- groups, whereas the anionic properties of CCA (Figure 1B) are attributed to SO_3^- and COO^- groups. The structures of CFB and CCA include OH groups bonded to the aromatic rings. CFB and CCA were investigated for the dispersion of MnO_2 in ethanol and EPD of MnO_2 films.

The suspensions of MnO_2 in ethanol were unstable and showed significant sedimentation 10 h after the ultrasonic

dx.doi.org/10.1021/jp304358q | J. Phys. Chem. B 2013, 117, 1563−1570

agitation. The addition of 0.05−0.15 g L^{-1} CCA or 0.05−0.8 g L^{-1} CFB to the MnO_2 suspensions resulted in reduced suspension stability. However, stable suspensions of MnO_2 were obtained at CCA concentrations of 0.3−0.8 g L^{-1}. Figure 2a,b shows 4 g L^{-1} MnO_2 suspensions without CCA and

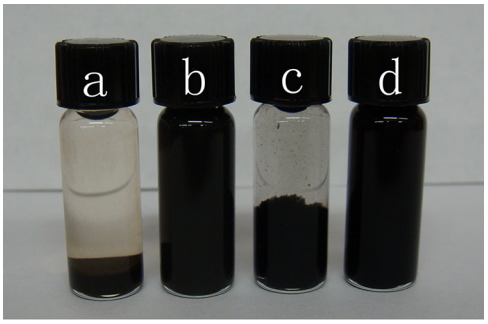

Figure 2. Suspensions of MnO_2 (a) without CCA and (b) containing CCA, and suspensions of MWCNT (c) without CCA and (d) containing CCA. Suspensions b and d were stable for more than 3 months.

containing 0.8 g L^{-1} CCA 3 months after the ultrasonic agitation. Figure 2b indicates excellent colloidal stability of the MnO_2 suspension, containing CCA. It is known that the formation of stable suspensions of MnO_2 nanoparticles with concentration above 1 mM (0.09 g L^{-1}) presents difficulties.[18] The dilute suspensions with MnO_2 concentration below 1 mM cannot be used for practical applications of EPD because the deposition rate in the EPD process is proportional to the particle concentration in the suspensions.[31] The use of CCA allowed the formation of stable suspensions of MnO_2 with a concentration of 1−10 g L^{-1}.

EPD from MnO_2 suspensions in ethanol resulted in the formation of cathodic deposits, indicating that MnO_2 particles were positively charged in the suspensions. However, as pointed out above, the suspensions exhibited very poor stability. As a result, the cathodic deposits obtained from the MnO_2 suspensions were nonuniform and contained agglomerated particles. The mechanism of inorganic particle charging in ethanol was discussed in the literature. Damodaran and Moudgil have proposed[32] a mechanism in which the alcohol, adsorbed on a particle, ionized into a protonated alcohol and an alkoxide ion, followed by the dissociation of the protonated alcohol. Pure alcohols can ionize in the following way:

$$RCH_2OH + RCH_2OH \rightarrow RCH_2O^- + RCH_2OH_2^+ \quad (2)$$

The dissociated alcohol and alkoxide ion desorbed into the solution, leaving a proton on the particle surface. This resulted in the formation of positively charged particles in the suspensions. This mechanism can also explain the positive charge of MnO_2 particles in ethanol suspensions.

The addition of CCA to MnO_2 suspensions resulted in the reduced cathodic deposition rate (Figure 3A) in the concentration range of 0−0.15 g L^{-1} CCA. However, anodic deposition was observed at higher CCA concentrations. The anodic deposition rate increased with increasing CCA concentration in the range of 0.15−0.8 g L^{-1} CCA. The anodic deposition resulted in the formation of uniform films. The addition of CFB to the MnO_2 suspensions resulted in a reduced deposition rate (Figure 3B) and no deposition, either cathodic or anodic, was observed at CFB concentrations higher than 0.05 g L^{-1}. The formation of anodic deposits from MnO_2

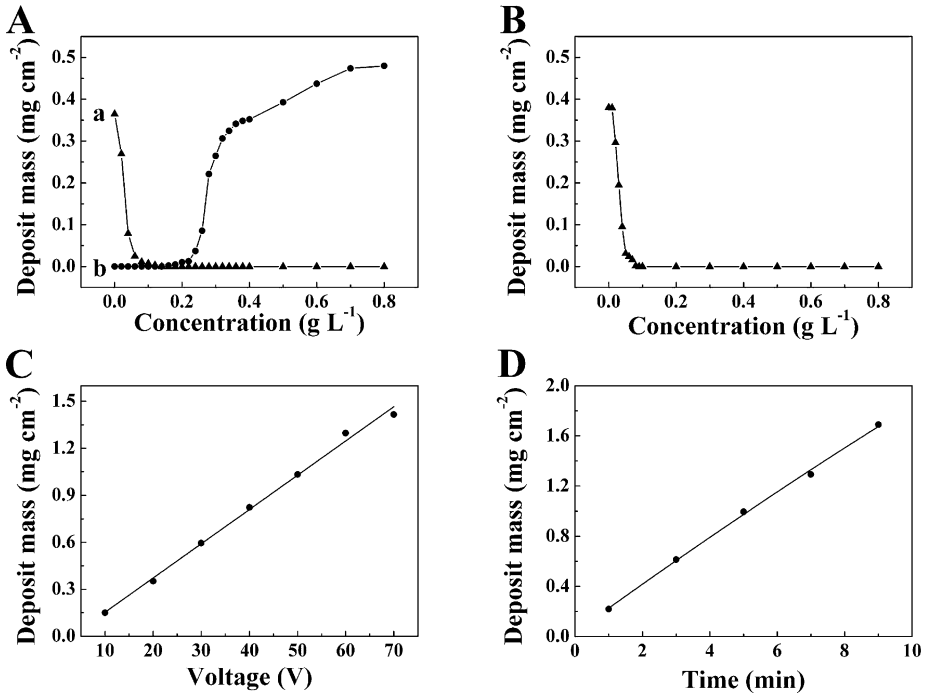

Figure 3. (A) deposit mass versus CCA concentration in the 4 g L^{-1} MnO_2 suspensions for (a) cathodic deposits and (b) anodic deposits at a deposition voltage of 20 V and deposition time of 2 min; (B) deposit mass versus CFB concentration in the 4 g L^{-1} MnO_2 suspensions for cathodic deposits at a deposition voltage of 20 V and deposition time of 2 min; (C) deposit mass versus deposition voltage for anodic deposits obtained from 4 g L^{-1} MnO_2 suspensions containing 0.4 g L^{-1} CCA for the deposition time of 2 min; (D) deposit mass versus deposition time for anodic deposits obtained from 4 g L^{-1} MnO_2 suspensions containing 0.4 g L^{-1} CCA at a deposition voltage of 20 V.

dx.doi.org/10.1021/jp304358q | J. Phys. Chem. B 2013, 117, 1563−1570

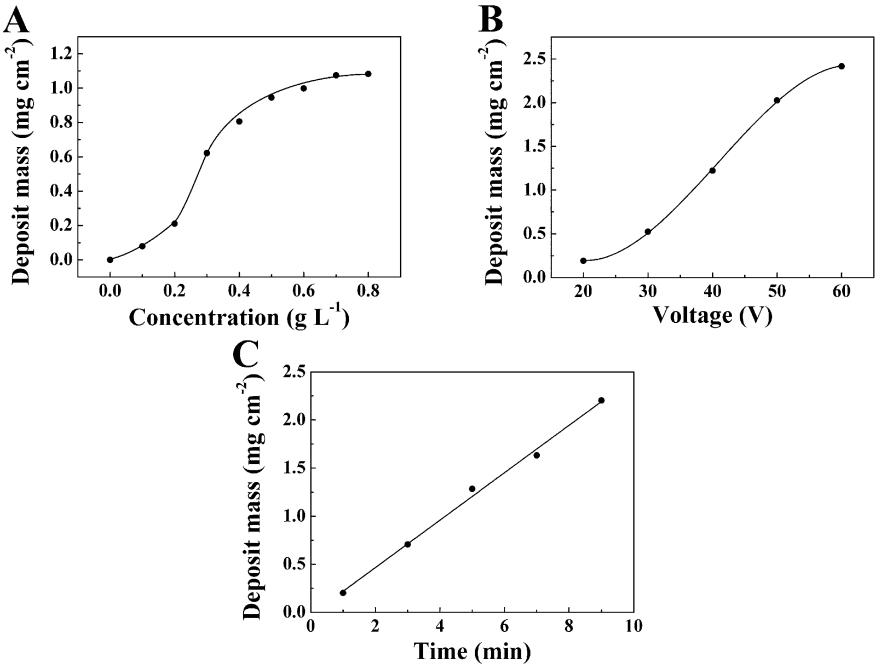

Figure 4. (A) Deposit mass versus CCA concentration in 1 g L^{-1} MWCNT suspension at a deposition voltage of 60 V and deposition time of 5 min.; (B) deposit mass versus deposition voltage for 1 g L^{-1} MWCNT suspension, containing 0.8 g L^{-1} CCA and deposition time of 10 min; (C) deposit mass versus deposition time for 1 g L^{-1} MWCNT suspension, containing 0.8 g L^{-1} CCA at a deposition voltage of 60 V.

suspensions, containing CCA, indicated that MnO_2 nanoparticles were negatively charged at CCA concentrations above 0.15 g L^{-1}. The film mass increased with increasing deposition voltage (Figure 3C) and deposition time (Figure 3D). Therefore, films of different mass can be obtained, and deposition yield can be controlled.

The reduction of the cathodic deposition yield with increase of CFB and CCA concentration in the range of 0−0.15 g L^{-1} can be attributed to the adsorption of anionic CFB and CCA on the positively charged MnO_2 particles and charge compensation. The electrostatic attraction of the anionic molecules and positively charged MnO_2 promoted the adsorption of the molecules on the particle surfaces. However, the electrostatic interactions cannot explain the charge reversal of the MnO_2 particles at CCA concentrations above 0.15 g L^{-1}. The electrostatic interactions of CFB and CCA with MnO_2 particles are governed by the COO^- and SO_3^- functional groups (Figure 1) of the organic molecules. The dissociation of the organic molecules resulted in the formation of corresponding anions and Na^+ or H^+. Therefore, a competitive adsorption of the anions and Na^+ or H^+ on the MnO_2 particles can be expected. However, only anionic CCA showed strong adsorption to the MnO_2 particles, which resulted in charge reversal and improved suspension stability. By contrast, the adsorption of CFB on MnO_2 nanoparticles was weak. As a result, no charge reversal was observed, and the suspensions were unstable. The comparison of the chemical structures of CFB and CCA (Figure 1) indicated that strong adsorption of CCA is attributed to the salicylate type of bonding,[33,34] involving COOH and OH groups. It should be noted that previous investigation[35] showed that the addition of benzoic acid (BA) to MnO_2 suspensions resulted in an increasing cathodic deposition rate. This was attributed to weak interaction of anionic COO^- groups of BA with MnO_2 nanoparticles and preferred adsorption of H^+ on the particle surface. The analysis of the experimental data for CCA, containing COOH and OH groups bonded to the aromatic ring, and BA[35] without OH groups, indicated that that OH groups play an important role in the adsorption of the CCA molecules. It is known that salicylic acid, containing COOH and OH groups bonded to adjacent carbon atoms of the aromatic ring, is a powerful complexing agent.[33,34] It is able to coordinate metals with complete deprotonation of the COOH and OH groups. Similar to salicylic acid, CCA was found to be a strong complexing agent, which was used for the voltammetric determination of Co, Cu, Ni, Ca, Zn, Pb, and Hf in solutions.[36,37] The suggested mechanism of salicylate-type bonding of CCA to MnO_2 particles is shown in Figure 1C. It involves the complexation of Mn atoms on the MnO_2 surface.

CCA was also investigated for the dispersion and deposition of MWCNT. The suspensions of MWCNT in ethanol were unstable and showed rapid sedimentation immediately after the ultrasonic agitation. No EPD was achieved from such suspensions. The addition of CCA allowed the formation of stable suspensions. Figure 2c,d compares the MWCNT suspensions without CCA and with CCA. The suspension, containing CCA, was stable for more than 3 months.

It is suggested that CCA adsorbed on the MWCNT and provided electrosteric stabilization. The chemical structure of the CCA molecules was beneficial for their adsorption on the MWCNT. It is in this regard that aromatic molecules are known[38−40] to interact strongly with sidewalls of CNTs through $\pi-\pi$ stacking. It was demonstrated[38] that the adsorption affinity of the phenolic molecules to CNT increased with the increasing number of aromatic rings and OH groups. As a result, 1-naphthol and pyrogallol showed better adsorption on CNT[38] compared to phenol. Small cationic and anionic aromatic molecules from the catechol and pyrogallol families were investigated for the EPD of MnO_2−MWCNT composites.[35,41] However, no EPD of pure MWCNT films was achieved. It was found that electric field promoted MWCNT aggregation and sedimentation. The electric field-induced

dx.doi.org/10.1021/jp304358q | J. Phys. Chem. B 2013, 117, 1563−1570

agglomeration was also observed during EPD of ceramic nanoparticles.[13] These investigations highlighted the importance of efficient dispersing agents for the application in electrophoretic nanotechnology.

A critical property of a dispersant is its adsorption on the material surface. Due to the strong adsorption of CCA on the MWCNT, the MWCNT suspensions showed excellent stability in an electric field. In contrast to the results of previous investigations of aromatic molecules from the catechol and pyrogallol families,[35,41] the use of CCA as a charging and dispersing agent allowed the formation of pure MWCNT films by EPD. The EPD method provided controlled deposition of MWCNT films. Figure4A shows film mass versus CCA concentration in suspensions. The increase in CCA concentration in the suspensions resulted in increasing deposition yield. The data indicated that the increase in the CCA concentration in the suspension resulted in an increasing amount of adsorbed CCA, which provided electrosteric stabilization and electric charge for EPD of MWCNT. The increase in the deposition voltage resulted in significant increase of the deposition yield (Figure4B). Relatively high deposition yield can be achieved at deposition voltages of 40−60 V. The deposit mass increased with increasing deposition time, indicating the formation of films of different mass (Figure 4C).

The results presented above indicated that CCA is an efficient dispersing and charging agent for EPD of two different materials: MnO_2 and MWCNT. The adsorption of CCA on MnO_2 and MWCNT was confirmed by the FTIR method. Figure 5 shows FTIR spectra for the deposits obtained from

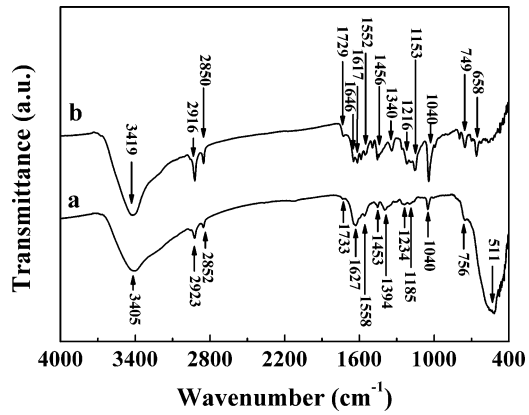

Figure 5. FTIR spectra of (a) a deposit prepared from 4 g L^{-1} MnO_2 suspensions containing 0.4 g L^{-1} CCA and (b) a deposit prepared from 1 g L^{-1} MWCNT suspensions containing 0.4 g L^{-1} CCA.

MnO_2 and MWCNT suspensions, containing CCA. The peak assignments are presented in Table 1. The FTIR spectrum of MnO_2 deposit showed absorptions attributed to stretching vibrations of the aromatic ring, SO_3^- group and other vibrations of adsorbed CCA. The SO_3^- vibrations of adsorbed CCA were observed in the spectrum of deposited MWCNT. The FTIR results confirmed that CCA was adsorbed on two different materials: MnO_2 and MWCNT. The CCA adsorption on MnO_2 was attributed to salicylate type of bonding. The mechanism of CCA adsorption on MWCNT was related to $\pi-\pi$ interactions.

The adsorbed CCA provided a charge, required for the electrophoresis of MnO_2 and MWCNT. The fundamental

Table 1. Band Assignments for MnO_2 and MWCNT Deposits Obtained Using CCA Additive[a]

MnO_2	MWCNT	band assignment
3405	3419	ν (O−H)[48]
2923, 2852	2916, 2850	ν (C−H)[48]
1733	1729	ν (C═O)[49]
1627, 1558	1646,1617,1552	ν (C−C)[50]
1453	1456	ν (C−C)[50,51]
1394, 1234	1340, 1216	δ (C−OH)[51]
1185	1153	ν (SO_3^-)[52,53]
1040	1040	ν (SO_3^-)[53,54]
756	749, 658	δ (C−H)[55]
511		ν (Mn−O)[56]

[a]The wavenumbers were given in cm^{-1}. ν = stretching mode; δ = bending mode.

aspects of electrophoresis of charged particles have been discussed in many investigations.[31,42] The concept of ζ potential was developed for hard particles. By contrast, the equations for electrophoretic mobility of polymers or ceramic nanoparticles, containing adsorbed organic molecules, do not include ζ potential.[43,44] It was shown that the concept of ζ potential, which is important in the electrokinetics of hard particles, loses its physical meaning in the electrokinetics of soft particles.[45] The high particle charge or high ζ potential of particles are important factors controlling suspension stability. However, high charge or high ζ potential of ceramic particles does not necessarily allow their EPD. The particles must coagulate at the electrode surface in order to form a film. It was shown that mutual repulsion of the charged particles or polymer macromolecules, accumulated at the electrode surface due to electrophoresis, can prevent their coagulation and deposition.[13] However, using CCA as a dispersing and charging agent, efficient deposition of MnO_2 and MWCNT was achieved. It is important to note that for ES applications, which depend on the electronic conductivity of CNTs, the use of CCA for MWCNT dispersion and charging offers advantages, because this approach does not introduce defects on the MWCNT sidewalls. This in contrast to other methods, which are based on CNT chemical functionalization[21] and oxidation in acidic solutions.[23,24]

The possibility of deposition of MnO_2 and MWCNT, using CCA as a dispersing agent for both materials, paves the way for the fabrication of composite MnO_2−MWCNT materials by EPD. The composite films were obtained from the suspensions containing MnO_2 and MWCNT, which were dispersed using CCA. The amount of MnO_2 and MWCNT in the suspensions was varied. Figure 6 shows deposit mass versus MWCNT concentration in the 2 g L^{-1} MnO_2 suspensions at a deposition voltage of 40 V and deposition time of 2 min. The addition of MWCNT to the MnO_2 suspension resulted in increased deposition yield, indicating codeposition of MnO_2 and MWCNT. The increase in MWCNT concentration in the suspensions in the range of 0−0.53 g L^{-1} resulted in continuous increase in the deposit mass in the range of 0.11−0.47 $mgcm^{-2}$, attributed to the increased amount of the deposited MWCNT. Therefore, the amount of MWCNT in the deposits can be varied. The deposit mass versus deposition time dependence (Figure 6B) showed linear increase of film mass, indicating the possibility of deposition of composite films of different mass.

The films prepared by the EPD method were investigated by SEM. Figure 7A shows a surface of the MnO_2 deposit. The

dx.doi.org/10.1021/jp304358q | J. Phys. Chem. B 2013, 117, 1563−1570

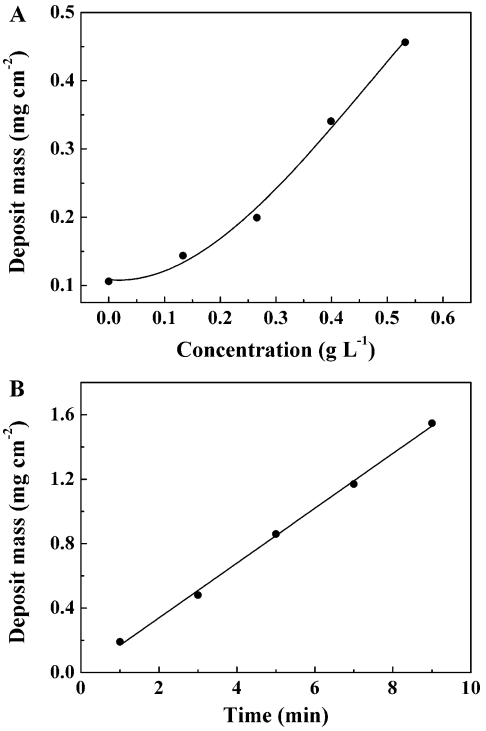

Figure 6. (A) Deposit mass versus MWCNT concentration in 2 g L^{-1} MnO_2 suspensions, containing 0.4 g L^{-1} CCA at a deposition voltage of 40 V and deposition time of 2 min; (B) deposit mass versus deposition time for 2 g L^{-1} MnO_2 suspensions, containing 0.4 g L^{-1} CCA and 0.5 g L^{-1} MWCNT at a deposition voltage of 40 V.

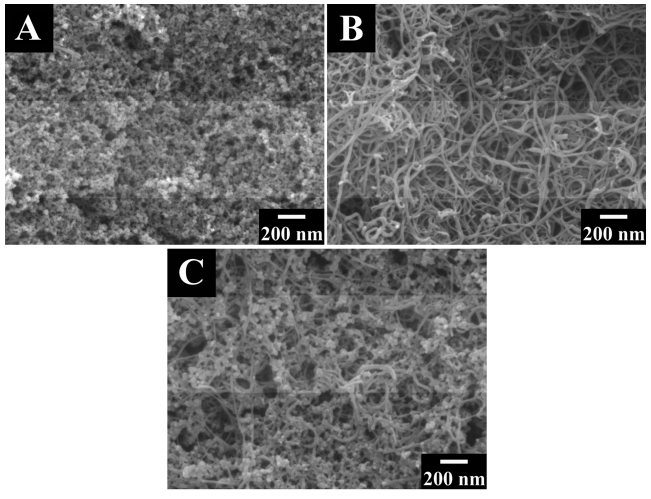

Figure 7. SEM images of films prepared from (A) 4 g L^{-1} MnO_2 suspensions, (B) 1 g L^{-1} MWCNT suspensions, and (C) 1 g L^{-1} MnO_2 suspensions, containing 0.13 g L^{-1} MWCNT.

deposit contained MnO_2 nanoparticles. The porosity can be attributed to packing of the particles and gas evolution at the electrode. Figure 7B shows a surface of a MWCNT deposit. The MWCNTs were nonagglomerated due to the use of CCA dispersant. The SEM images of the deposits prepared from MnO_2 suspensions, containing MWCNT, showed that the deposits contained MnO_2 particles and MWCNT. A typical image of a composite MnO_2–MWCNT film is shown in Figure 7C.

The formation of composite films was confirmed by TGA and DTA studies. Figure 8 shows TGA and DTA data for the

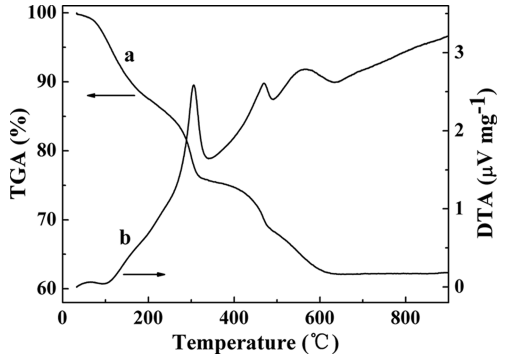

Figure 8. (a)TGA and (b) DTA data for the deposit obtained from 1 g L^{-1} MnO_2 suspensions, containing 0.13 g L^{-1} MWCNT at a constant voltage of 40 V.

deposit, prepared from the 1 g L^{-1} MnO_2 suspension, containing 0.13 g L^{-1} MWCNT and 0.2 g L^{-1} CCA. The TGA data showed several steps in mass loss below 600 °C. The mass loss below 200 °C can be mainly attributed to dehydration. The corresponding DTA data showed a broad endotherm centered at 100 °C. The mass loss at higher temperatures can be mainly attributed to burning out of MWCNT. However, the mass loss can be partially attributed to burning out of CCA, which was adsorbed on MnO_2 particles and MWCNT and incorporated into the deposit. The DTA data showed exothermic peaks at 305, 467, and 556 °C, which corresponded to different steps in mass loss. The total mass loss at 700 °C was found to be 38% of the initial sample mass, indicating that MnO_2 content in the composite material was 62%.

The composite films prepared by EPD were investigated for application in ES. The charge–discharge behavior of MnO_2 is given by the following reaction:[46]

$$MnO_2 + A^+ + e^- \leftrightarrow MnO_2A \quad (3)$$

where $A^+ = Li^+, Na^+, K^+, H^+$. Equation 3 indicates that high electronic and ionic conductivities are necessary in order to utilize capacitive properties of MnO_2. The incorporation of MWCNT into the MnO_2 matrix allowed improved electronic conductivity of the composite material. The porous structure of the composite was beneficial for Na^+ ion access from the electrolyte to the MnO_2 particles. Figure 9 compares capacitive behavior of the MnO_2 and composite films. The box shape of

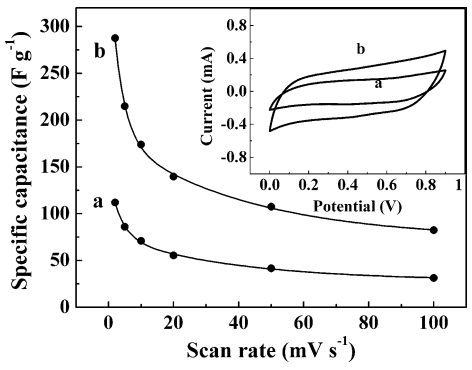

Figure 9. SC versus scan rate and (inset) corresponding CVs at 10 mVs^{-1} for the films, prepared from 1 g L^{-1} MnO_2 suspensions, containing 0.2 g L^{-1} CCA (a) without MWCNT and (b) with 0.13 g L^{-1} MWCNT, sample mass 0.15 mg cm^{-2}.

dx.doi.org/10.1021/jp304358q | J. Phys. Chem. B 2013, 117, 1563–1570

the CVs indicated capacitive properties of the films in the voltage window of 0−0.9 V. The larger area of the CV of the composite film was attributed to higher SC, compared to pure MnO_2 film. The SC calculated from the CV data decreased with increasing scan rate due to the electrolyte diffusion limitations in the pores of the materials. The composite material showed higher SC in the scan rate of 2−100 mV s^{-1} compared to SC of pure MnO_2 films. The highest SC of 290 Fg^{-1} (44 $mFcm^{-2}$) was obtained at a scan rate of 2 mV s^{-1}. The SC of electrodes of similar mass prepared by other methods is usually[46] in the range of 200−300 Fg^{-1}. Impedance spectroscopy data for the MnO_2−MWCNT composite and pure MnO_2 films are presented in Figure 10. The Nyquist plots for the

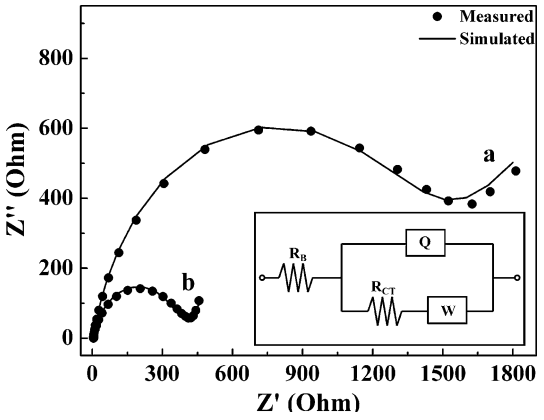

Figure 10. Nyquist plot of complex impedance $Z = Z' - iZ''$ for the films, prepared from 1 g L^{-1} MnO_2 suspensions, containing 0.2 g L^{-1} CCA (a) without MWCNT and (b) with 0.13 g L^{-1} MWCNT, sample mass 0.15 $mgcm^{-2}$; inset shows equivalent circuit used for simulation.

complex impedance $Z = Z' - iZ''$ showed significantly lower impedance values for composite films, compared to the corresponding values for pure MnO_2 films. The equivalent circuit[47] of the films included bulk electrolyte resistance (R_B), capacitance, represented by a constant phase element (Q), charge transfer resistance (R_{CT}) and Warburg element (W). The lower impedance of the composite films, containing MWCNT, resulted in higher SC (Figure 9). The R_{CT} values were found to be 1420 and 36 Ohm for pure MnO_2 and composite MnO−-MWCNT films, respectively. The results showed the beneficial effect of MWCNT. However, further optimization of the deposition conditions and deposit composition would be beneficial for the fabrication of MnO_2−MWCNT composite electrodes for ES. The approach developed in this investigation can be used for the fabrication of other composites containing oxide nanoparticles and CNT.

CONCLUSIONS

A new EPD method has been developed for the fabrication of MnO_2−MWCNT composites. CCA showed strong adsorption on MWCNT, allowed good MWCNT dispersion in the bulk of suspensions and controlled EPD of MWCNT films. The adsorption of CCA on MnO_2 nanoparticles allowed the formation of concentrated suspensions of well dispersed MnO_2 nanoparticles particles and fabrication of MnO_2 films. The mechanism of CCA adsorption on MWCNT was related to $\pi-\pi$ interactions. The CCA adsorption on MnO_2 was attributed to salicylate type of bonding. It was found that CCA can be used as a dispersing and charging agent for EPD of two different types of materials: MWCNT and MnO_2. Composite MnO_2−MWCNT films prepared by EPD showed capacitive behavior in the 0.5 M Na_2SO_4 aqueous electrolyte. The composite films showed higher SC compared to SC of pure MnO_2 films. The improved capacitive behavior was attributed to lower impedance of the composite films. The composite films showed a SC of 290 F g^{-1} and can be used for the fabrication of electrodes of ES. The EPD method developed in this investigation can be utilized for the fabrication of other composites containing ceramic particles and CNTs.

AUTHOR INFORMATION

Corresponding Author

*Phone 905-525-9140 ext. 23914; e-mail: zhitom@mcmaster.ca.

Notes

The authors declare no competing financial interest.

ACKNOWLEDGMENTS

The authors gratefully acknowledge the financial support of the Natural Sciences and Engineering Research Council of Canada.

REFERENCES

(1) Mayen-Mondragon, R.; Falk, G.; Clasen, R. *J. Am. Ceram. Soc.* **2012**, *95*, 593−599.
(2) Boccaccini, A. R.; Zhitomirsky, I. *Curr. Opin. Solid State Mater. Sci.* **2002**, *6*, 251−260.
(3) Boccaccini, A. R.; Keim, S.; Ma, R.; Li, Y.; Zhitomirsky, I. *J. R. Soc. Interface* **2010**, *7*, S581−S613.
(4) Van Der Biest, O.; Joos, E.; Vleugels, J.; Baufeld, B. *J. Mater. Sci.* **2006**, *41*, 8086−8092.
(5) Nold, A.; Zeiner, J.; Assion, T.; Clasen, R. *J. Eur. Ceram. Soc.* **2010**, *30*, 1163−1170.
(6) Somarajan, S.; Hasan, S. A.; Adkins, C. T.; Harth, E.; Dickerson, J. H. *J. Phys. Chem. B* **2008**, *112*, 23−28.
(7) Ferrari, B.; Moreno, R. *J. Eur. Ceram. Soc.* **2010**, *30*, 1069−1078.
(8) Besra, L.; Liu, M. *Prog. Mater. Sci.* **2007**, *52*, 1−61.
(9) Groenewold, J.; Zhang, T.; Kegel, W. K. *J. Phys. Chem. B* **2011**, *115*, 7264−7267.
(10) Carrique, F.; Ruiz-Reina, E.; Arroyo, F. J.; Delgado, A. V. *J. Phys. Chem. B* **2010**, *114*, 6134−6143.
(11) Boccaccini, A. R.; Roether, J. A.; Thomas, B. J. C.; Shaffer, M. S. P.; Chavez, E.; Stoll, E.; Jane Minay, E. *J. Ceram. Soc. Japan* **2006**, *114*, 1−14.
(12) Hasan, S. A.; Kavich, D. W.; Mahajan, S. V.; Dickerson, J. H. *Thin Solid Films* **2009**, *517*, 2665−2669.
(13) Zhitomirsky, I. *Adv. Colloid Interface Sci.* **2002**, *97*, 277−315.
(14) Wu, K.; Wang, Y.; Zhitomirsky, I. *J. Colloid Interface Sci.* **2010**, *352*, 371−378.
(15) Boccaccini, A. R.; Cho, J.; Subhani, T.; Kaya, C.; Kaya, F. *J. Eur. Ceram. Soc.* **2010**, *30*, 1115−1129.
(16) Boccaccini, A. R.; Cho, J.; Roether, J. A.; Thomas, B. J. C.; Jane Minay, E.; Shaffer, M. S. P. *Carbon* **2006**, *44*, 3149−3160.
(17) Mahajan, S. V.; Cho, J.; Shaffer, M. S. P.; Boccaccini, A. R.; Dickerson, J. H. *J. Eur. Ceram. Soc.* **2010**, *30*, 1145−1150.
(18) Chin, S.-F.; Pang, S.-C.; Anderson, M. A. *J. Electrochem. Soc.* **2002**, *149*, A379−A384.
(19) Li, J.; Yang, Q. M.; Zhitomirsky, I. *J. Power Sources* **2008**, *185*, 1569−1574.
(20) Grandfield, K.; Sun, F.; FitzPatrick, M.; Cheong, M.; Zhitomirsky, I. *Surf. Coat. Technol.* **2009**, *203*, 1481−1487.
(21) Casagrande, T.; Lawson, G.; Li, H.; Wei, J.; Adronov, A.; Zhitomirsky, I. *Mater. Chem. Phys.* **2008**, *111*, 42−49.
(22) Wu, K.; Imin, P.; Sun, Y.; Pang, X.; Adronov, A.; Zhitomirsky, I. *Mater. Lett.* **2012**, *67*, 248−251.

(23) Vaisman, L.; Wagner, H. D.; Marom, G. *Adv. Colloid Interface Sci.* **2006**, *128*−*130*, 37−46.
(24) Esumi, K.; Ishigami, M.; Nakajima, A.; Sawada, K.; Honda, H. *Carbon* **1996**, *34*, 279−281.
(25) Thomas, B. J. C.; Boccaccini, A. R.; Shaffer, M. S. P. *J. Am. Ceram. Soc.* **2005**, *88*, 980−982.
(26) Du, C.; Pan, N. *Nanotechnology* **2006**, *17*, 5314−5318.
(27) Zhu, G.; Pan, L.; Lu, T.; Liu, X.; Lv, T.; Xu, T.; Sun, Z. *Electrochim. Acta* **2011**, *56*, 10288−10291.
(28) Nie, C.; Pan, L.; Liu, Y.; Li, H.; Chen, T.; Lu, T.; Sun, Z. *Electrochim. Acta* **2012**, *66*, 106−109.
(29) Grandfield, K.; Sun, F.; FitzPatrick, M.; Cheong, M.; Zhitomirsky, I. *Surf. Coat. Technol.* **2009**, *203*, 1481−1487.
(30) Cheong, M.; Zhitomirsky, I. *Surf. Eng.* **2009**, *25*, 346−352.
(31) Van der Biest, O. O.; Vandeperre, L. J. *Annu. Rev. Mater. Sci.* **1999**, *29*, 327−352.
(32) Damodaran, R.; Moudgil, B. M. *Colloid. Surf. A* **1993**, *80*, 191−195.
(33) Dobson, K. D.; McQuillan, A. J. *Spectrochim. Acta A* **2000**, *56*, 557−565.
(34) Tunesi, S.; Anderson, M. A. *Langmuir* **1992**, *8*, 487−495.
(35) Wang, Y.; Zhitomirsky, I. *Colloid. Surf. A* **2010**, *369*, 211−217.
(36) Levytska, H.; Orshuliak, O. *Talanta* **2007**, *71*, 1441−1443.
(37) Kocjan, R.; Bazewicz, A.; Blicharska, E. *J. Sep. Sci.* **2002**, *25*, 891−896.
(38) Lin, D.; Xing, B. *Environ. Sci. Technol.* **2008**, *42*, 7254−7259.
(39) Woods, L. M.; Badescu, S. C.; Reinecke, T. L. *Phys. Rev. B* **2007**, *75*, 155415−155419.
(40) Star, A.; Han, T.-R.; Gabriel, J.-C. P.; Bradley, K.; Gruner, G. *Nano Lett.* **2003**, *3*, 1421−1423.
(41) Wang, Y.; Zhitomirsky, I. *Langmuir* **2009**, *25*, 9684−9689.
(42) Sarkar, P.; Nicholson, P. S. *J. Am. Ceram. Soc.* **1996**, *79*, 1987−2002.
(43) Ohshima, H. *Colloid. Surf. A* **1995**, *103*, 249−255.
(44) Ohshima, H. *J. Colloid Interface Sci.* **2001**, *233*, 142−152.
(45) Ohshima, H. *Sci. Technol. Adv. Mater.* **2009**, *10*, 063001.
(46) Devaraj, S.; Munichandraiah, N. *Electrochem. Solid State Lett.* **2005**, *8*, A373−A377.
(47) Jo, C.; Hwang, I.; Lee, J.; Lee, C. W.; Yoon, S. *J. Phys. Chem. C* **2011**, *115*, 11880−11886.
(48) Rajh, T.; Chen, L. X.; Lukas, K.; Liu, T.; Thurnauer, M. C.; Tiede, D. M. *J. Phys. Chem. B* **2002**, *106*, 10543−10552.
(49) Liu, G.; Wu, T.; Zhao, J.; Hidaka, H.; Serpone, N. *Environ. Sci. Technol.* **1999**, *33*, 2081−2087.
(50) Weisz, A. D.; Garcia Rodenas, L.; Morando, P. J.; Regazzoni, A. E.; Blesa, M. A. *Catal. Today* **2002**, *76*, 103−112.
(51) Jankovic, I. A.; Saponjic, Z. V.; Comor, M. I.; Nedeljkovic, J. M. *J. Phys. Chem. C* **2009**, *113*, 12645−12652.
(52) Santos, L. R. B.; Chartier, T.; Pagnoux, C.; Baumard, J. F.; Santillii, C. V.; Pulcinelli, S. H.; Larbot, A. *J. Eur. Ceram. Soc.* **2004**, *24*, 3713−3721.
(53) Jayaweera, P. M.; Jayarathne, T. A. U. *Surf. Sci.* **2006**, *600*, L297−L300.
(54) Guedes, M.; Ferreira, J. M. F.; Ferro, A. C. *J. Colloid Interface Sci.* **2009**, *330*, 119−124.
(55) Kawaguti, C. A.; Santilli, C. V.; Pulcinelli, S. H. *J. Non-Cryst. Solid.* **2008**, *354*, 4790−4794.
(56) Yang, R.; Wang, Z.; Dai, L.; Chen, L. *Mater. Chem. Phys.* **2005**, *93*, 149−153.